A

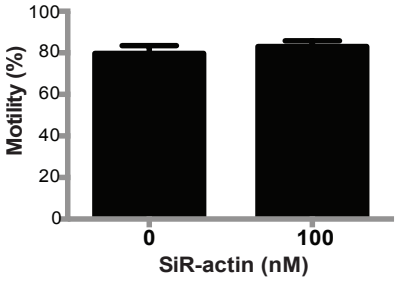

B

SiR-actin [nM]	0			100			P value
	Mean		SEM	Mean		SEM	
Curvilinear velocity (VCL) [µm/s]	113.5	±	17.3	99.7	±	13.1	0.56
Straight line velocity (VSL) [µm/s]	35.4	±	7.2	32.4	±	6.3	0.77
Average path velocity (VAP) [µm/s]	61.4	±	8.4	53.8	±	6.5	0.51
Linearity (LIN) [%]	30.8	±	2.0	31.9	±	2.3	0.73
Righteousness movement (STR) [%]	56.6	±	4.1	59.1	±	5.5	0.73
Amplitude of lateral head displacement (ALH) [µm]	3.6	±	0.5	3.3	±	0.3	0.66
Beat cross frequency (BCF) [Hz]	7.9	±	0.5	6.7	±	0.8	0.29

Figure S1. Motility and motion parameters of sperm loaded with SiR-actin. (A) Total motility of sperm loaded with 100 nM SiR-actin or vehicle (DMSO) obtained by CASA. Student´s t-test. n=3. At least 300 cells analyzed. P value=0.52. **(B)** Cinematic parameters obtained by CASA. Student´s t-test. n=3. At least 300 cells analyzed.

Journal of Cell Science • Supplementary information

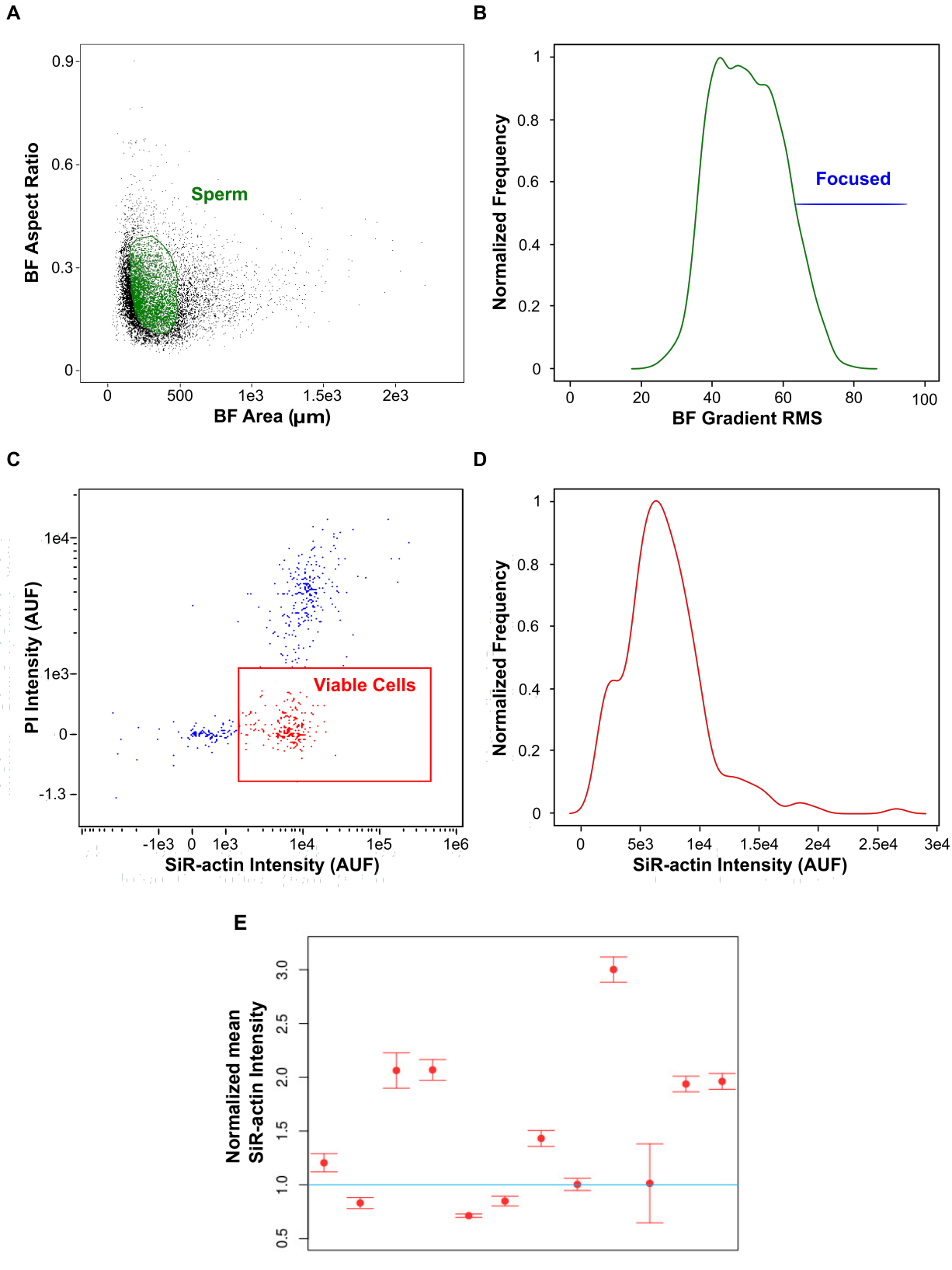

Journal of Cell Science • Supplementary information

Figure S2. Selection of the sperm population using image-based flow cytometry. Representative plots used to select the population of interest for SiR-actin fluorescence analysis in the different conditions. **(A)** Dot plot of Brightfield Area (BF Area (μm^2) versus Brightfield Aspect Ratio (BF Aspect Ratio) parameters to select the single sperm cells and to discriminate them from cell aggregates and debris. **(B)** Histogram of Gradient RMS in BF (Ch01) to exclude out-of-focus cells. **(C)** Dot plot of PI fluorescence intensity (Ch05) versus SiR-actin fluorescence intensity (Ch11) to select the alive sperm population (viable cells). AUF: Arbitrary Units of Fluorescence. **(D)** Histogram of SiR-actin fluorescence intensity in the population of interest with all previous discriminations. AUF: Arbitrary Units of Fluorescence. **(E)** Each dot represents SiR-actin mean fluorescence intensity ± SEM of the capacitated sperm population normalized with the SiR-actin mean fluorescence intensity of the paired non-capacitated sperm population (n=12 mice). Statistical analysis was performed using a Wilcoxon signed rank test. P value=0.014. The blue line represents the non-capacitated sperm population.

Journal of Cell Science • Supplementary information

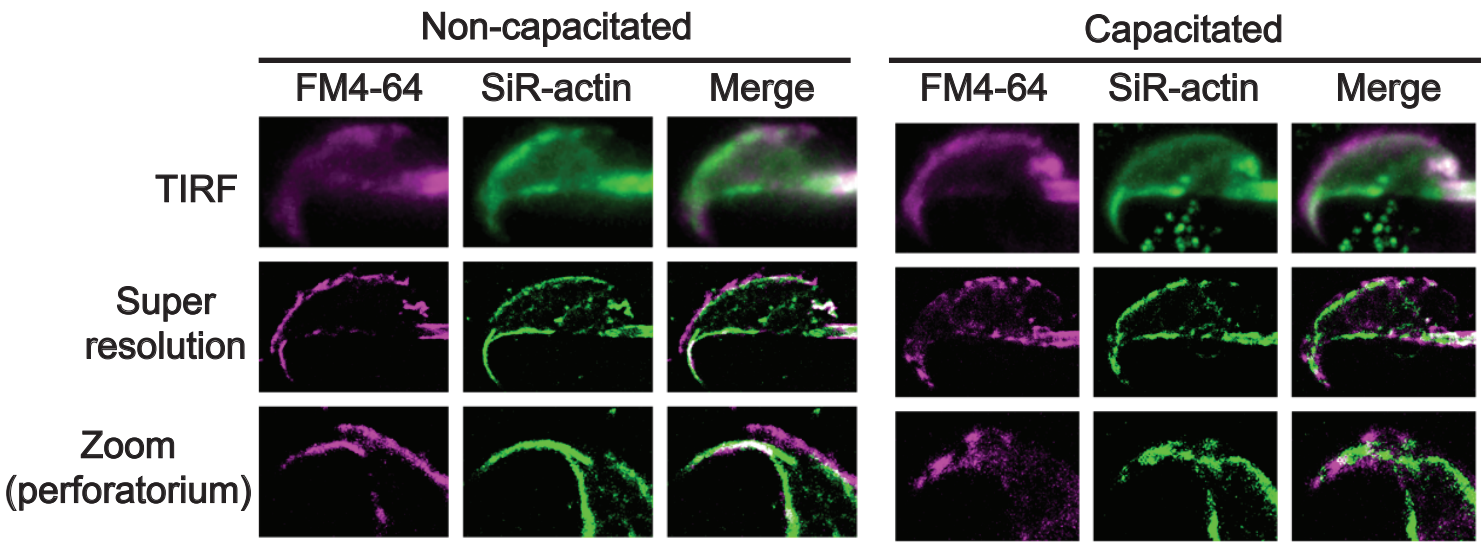

Figure S3. **The perforatorium F-actin cytoskeleton undergoes structural modifications during capacitation.** Representative images obtained by TIRF microscopy of a non-capacitated and a capacitated sperm loaded with SiR-actin and FM4-64. Its super-resolution SRRF reconstructions are shown. A zoom of the perforatorium area is shown, n=3, 10 cells analyzed.

Journal of Cell Science • Supplementary information

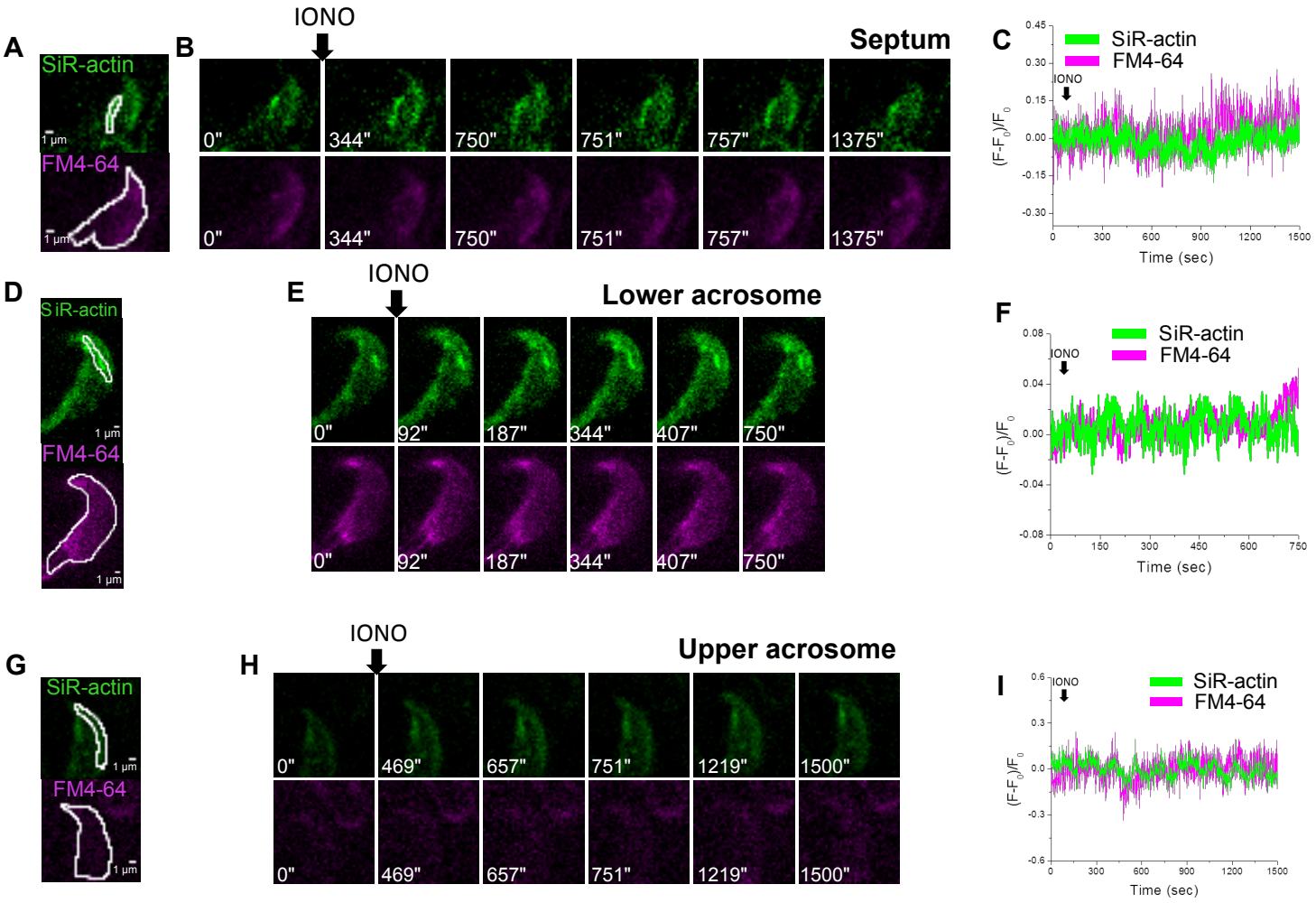

Figure S4. **Specific F-actin structures in the sperm head did not change in acrosome intact sperm.** Sperm were loaded with SiR-actin (green) and FM4-64 (magenta) and attached to concanavalin A-coated slides for imaging using TIRF microscopy. Following image acquisition, the ROIs indicated in **A, D and G** were analyzed. Representative image sequences of sperm stimulated with ionomycin that initially possessed the F-actin structure corresponding to the septum **(B)**, lower acrosome **(E)** or neck **(H)** region. The corresponding fluorescence traces **(C, F and I)** of the indicated ROIs (for SiR-actin) and the whole sperm head (for FM4-64) **(A, D and G)** are shown on the right. Analysis of these traces demonstrates that these structures remained intact in sperm that did not undergo AR in response to 10 µM of ionomycin. (n=6; 62 cells analyzed).

Journal of Cell Science • Supplementary information

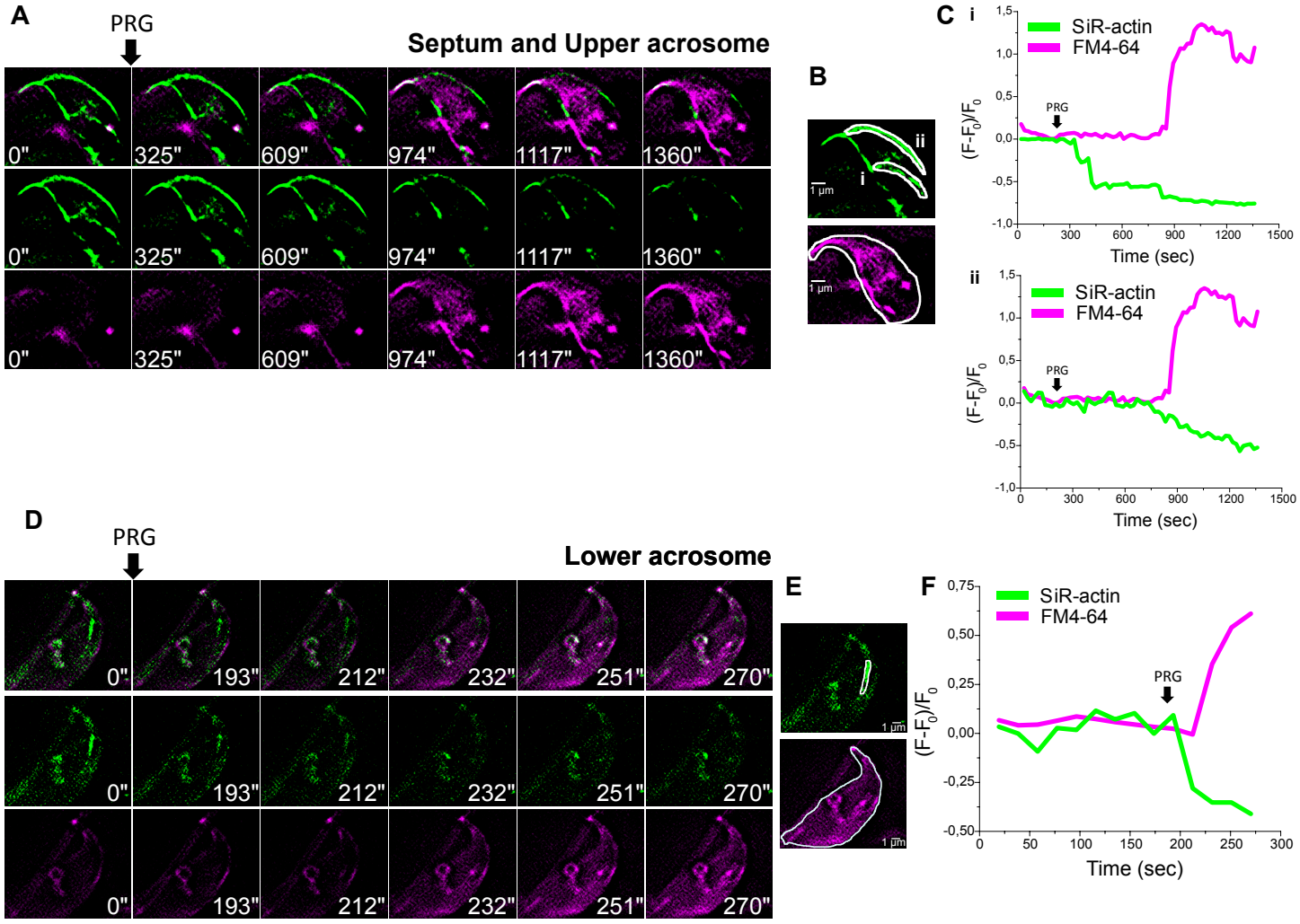

Figure S5. Specific dynamic changes in the actin cytoskeleton during progesterone-induced acrosomal exocytosis. Sperm were loaded with SiR-actin (green) and FM4-64 (magenta) and attached to concanavalin A-coated slides for imaging using TIRF microscopy. Following acquisition, images were analyzed using 3B analysis. **(A)** Representative super-resolution image sequence of a sperm which at the beginning of the recording possesses the septum and the upper acrosome F-actin structure previously described (left). The time course sequence of that structure after addition of progesterone is shown. The F-actin structure in the septum region depolymerizes prior to the initiation of the AR. On the other hand, the loss of F-actin in the upper acrosome occurred during the initiation of the AR as judged by the increase in FM4-64 fluorescence. **(B)** The ROIs corresponding to the septum region (i) and the upper acrosome (ii) (for SiR-actin) and the whole sperm head (for FM4-64) are shown together with the corresponding fluorescence traces **(C)**. **(D)** Representative super-resolution images of a sperm that undergoes actin de-polymerization in the lower acrosome region after stimulation with progesterone prior to the initiation of the AR. **(E)** The ROIs corresponding to the lower acrosome region (for SiR-actin) and the whole sperm head (for FM4-64) are shown together with the corresponding fluorescence traces **(F)**. (n=5; 28 cells analyzed).

Journal of Cell Science • Supplementary information

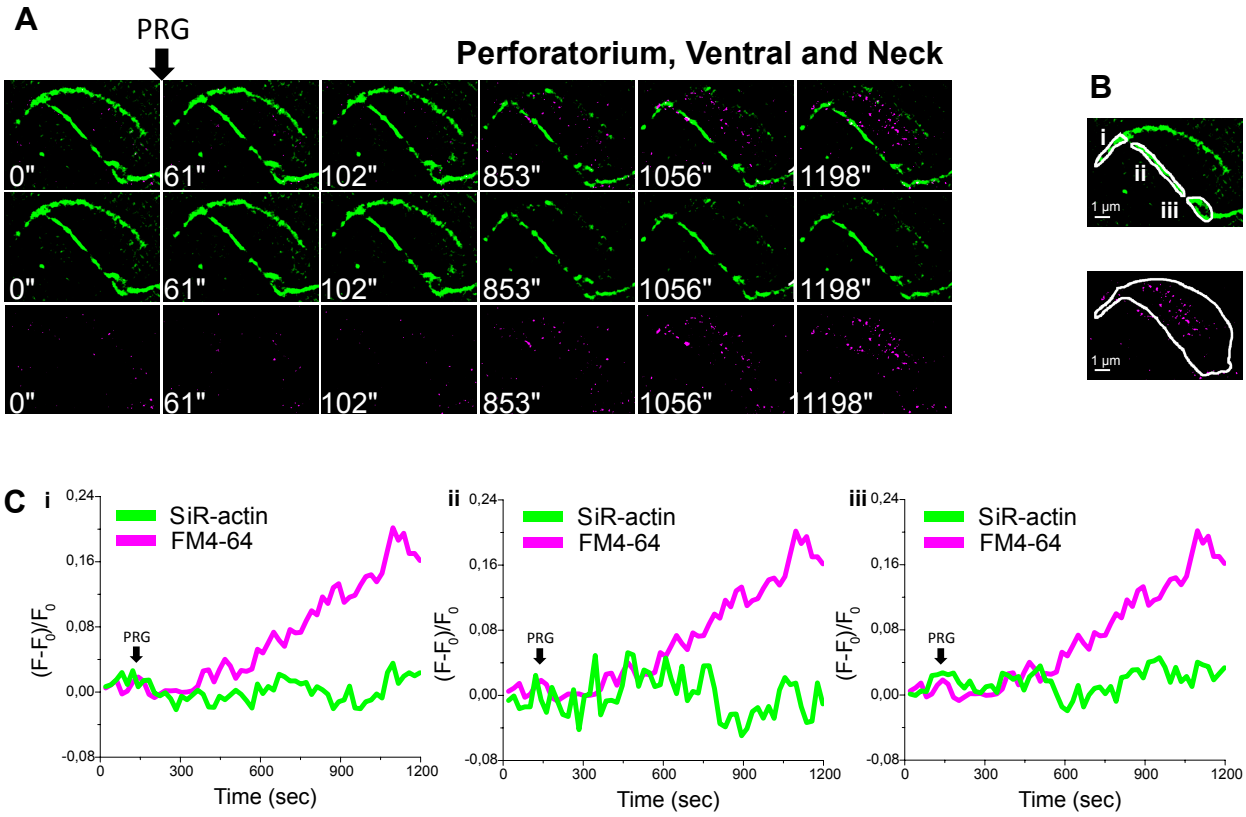

Figure S6. **Specific F-actin structures in the sperm head did not change as a consequence of the occurrence of the AR induced with progesterone.** Sperm were loaded with SiR-actin (green) and FM4-64 (magenta) and attached to concanavalin A-coated slides for imaging using TIRF microscopy. Following acquisition, images were analyzed using 3B analysis. **(A)** Representative super resolution image sequences of a sperm stimulated with progesterone that initially possessed the F-actin structure corresponding to the perforatorium (i), ventral (ii) or neck (iii) region. The ROIs indicated in (**B)** were analyzed. The corresponding fluorescence traces of the indicated ROIs (for SiR-actin) and the whole sperm head (for FM4-64) are shown in **(C)**. These fluorescence traces demonstrate that these structures remained intact in sperm that underwent AR. (n=5. 28 cells analyzed).

Journal of Cell Science • Supplementary information

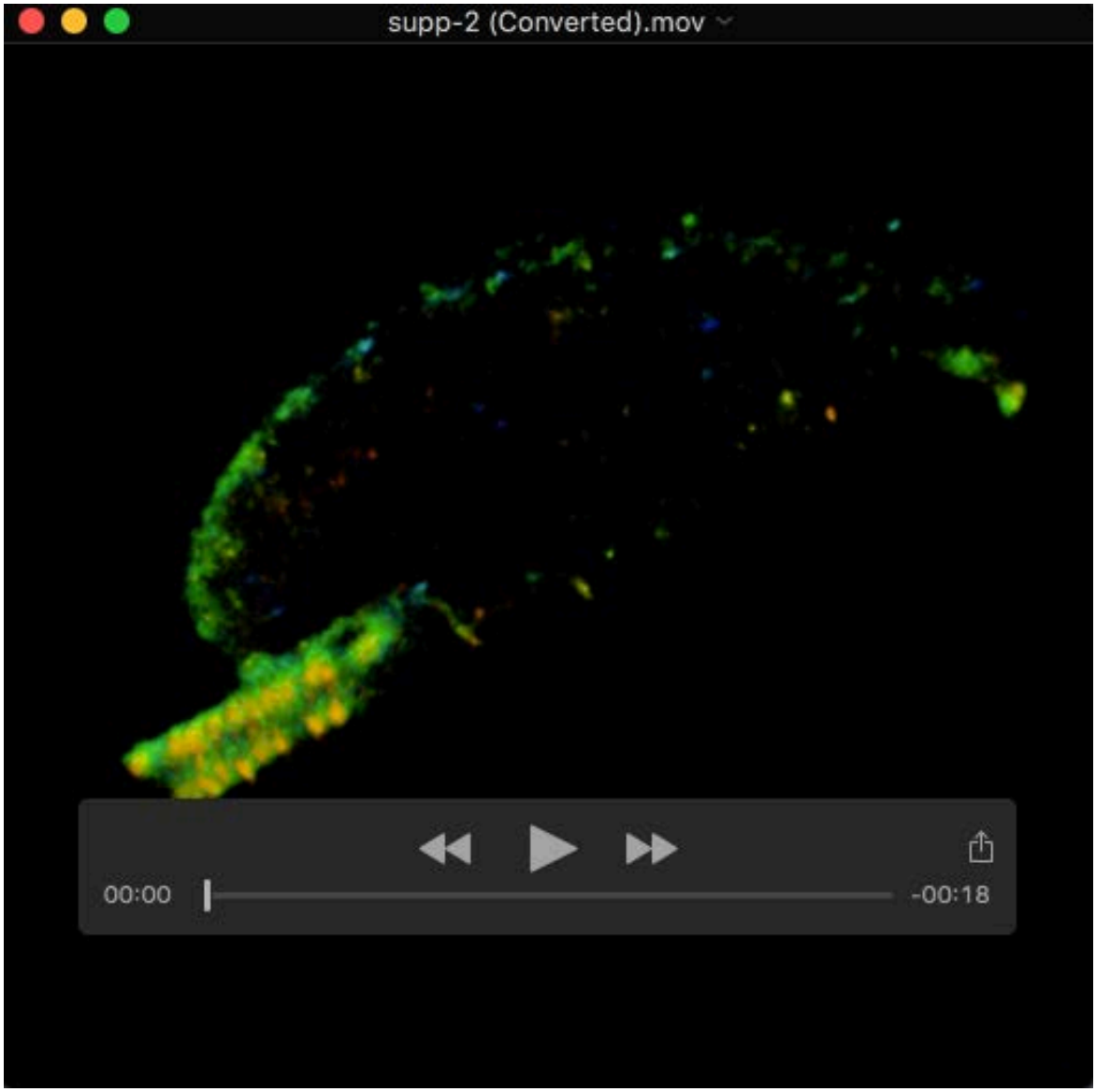

Movie S1: 3D STORM representations of phalloidin on the sperm head. The viewing angle is rotated around the *x*-axis. The *z*-position is color-coded according to the scale bar shown at the bottom right. Scale bar 500 nm. Related to **Figure 3B**.

Journal of Cell Science • Supplementary information

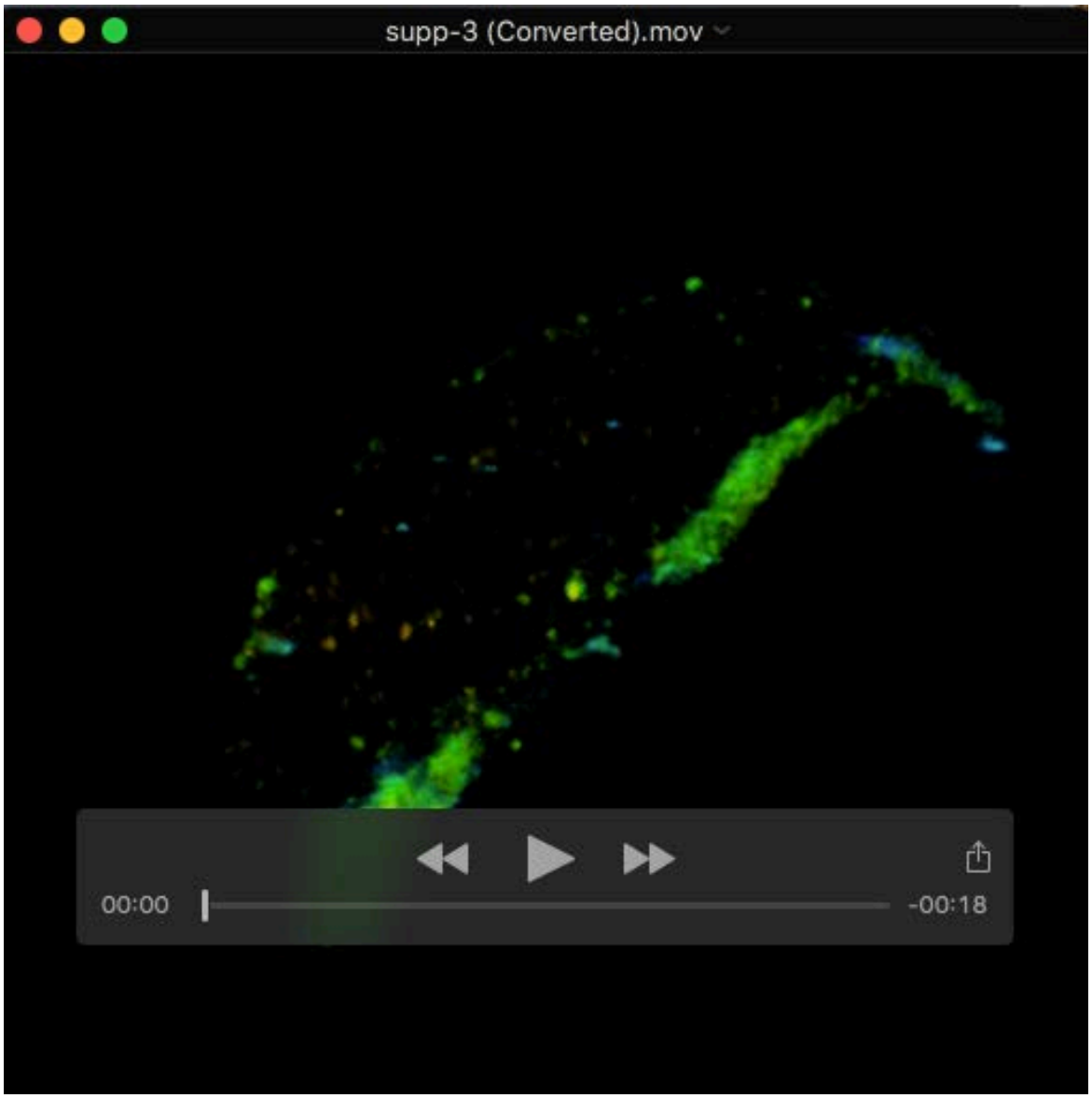

Movie S2: 3D STORM representations of phalloidin on the sperm head. The viewing angle is rotated around the *x*-axis. The *z*-position is color-coded according to the scale bar shown at the bottom right. Scale bar 500 nm. Related to **Figure 3B**.

Journal of Cell Science • Supplementary information

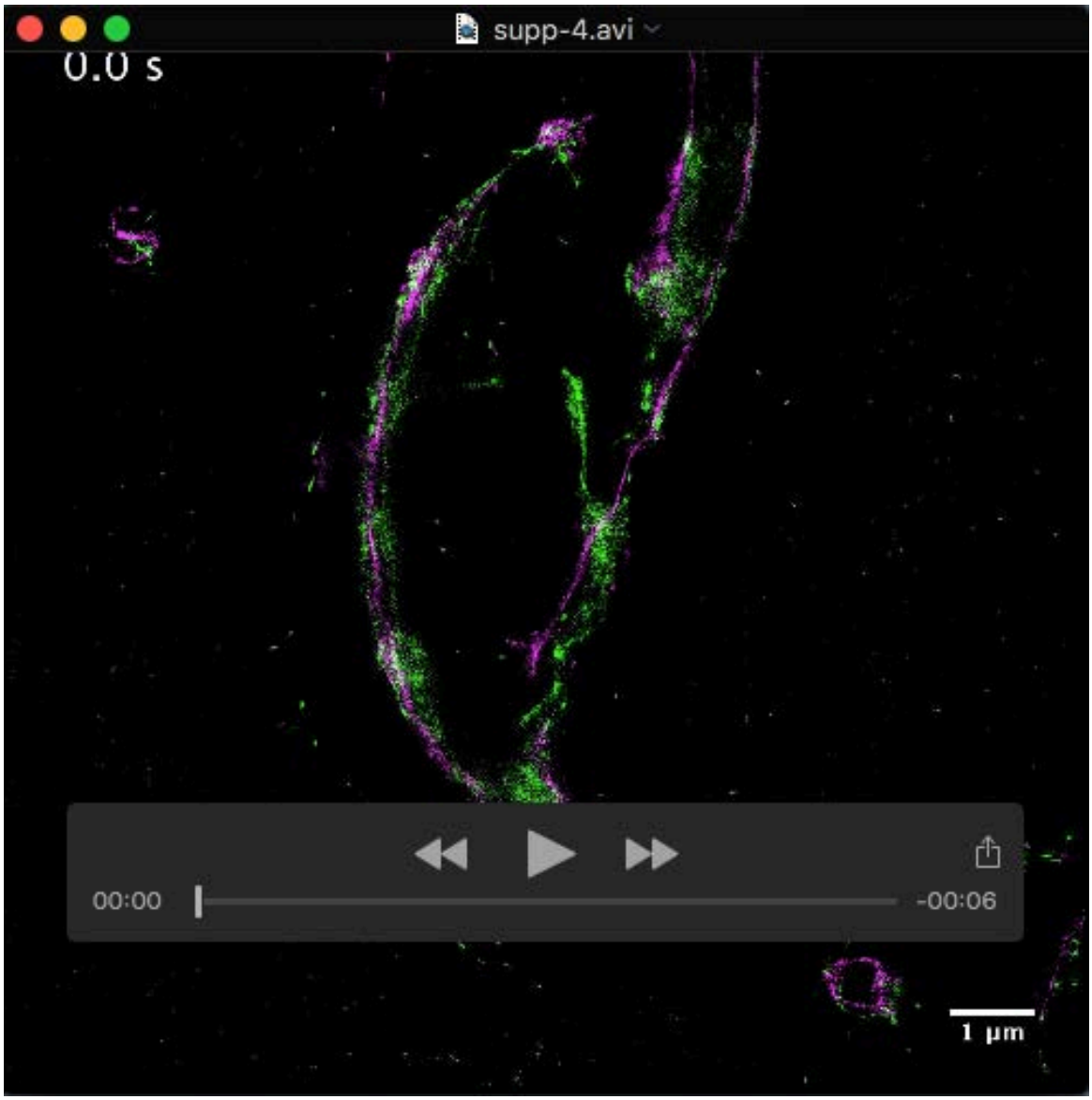

Movie S3: Representative super-resolution movie of a sperm, which at the beginning of the recording possesses the septum F-actin structure. The F-actin structure in the septum region de-polymerizes prior to the initiation of the AR after addition of 10 µM ionomycin. Related to **Figure 5A**.

Journal of Cell Science • Supplementary information

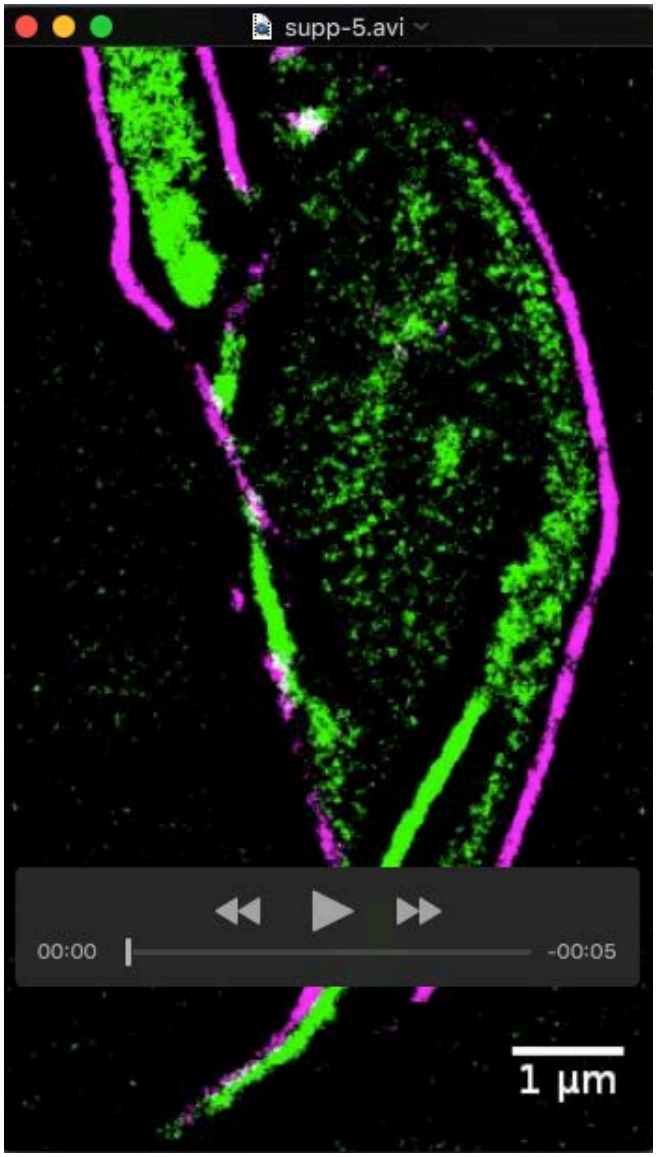

Movie S4: Representative super-resolution movie of a sperm, which at the beginning of the recording possesses the lower acrosome F-actin structure. The F-actin structure in the lower acrosome region de-polymerizes prior to the initiation of the AR after the addition of 10 µM ionomycin. Related to **Figure 5D**.

Journal of Cell Science • Supplementary information

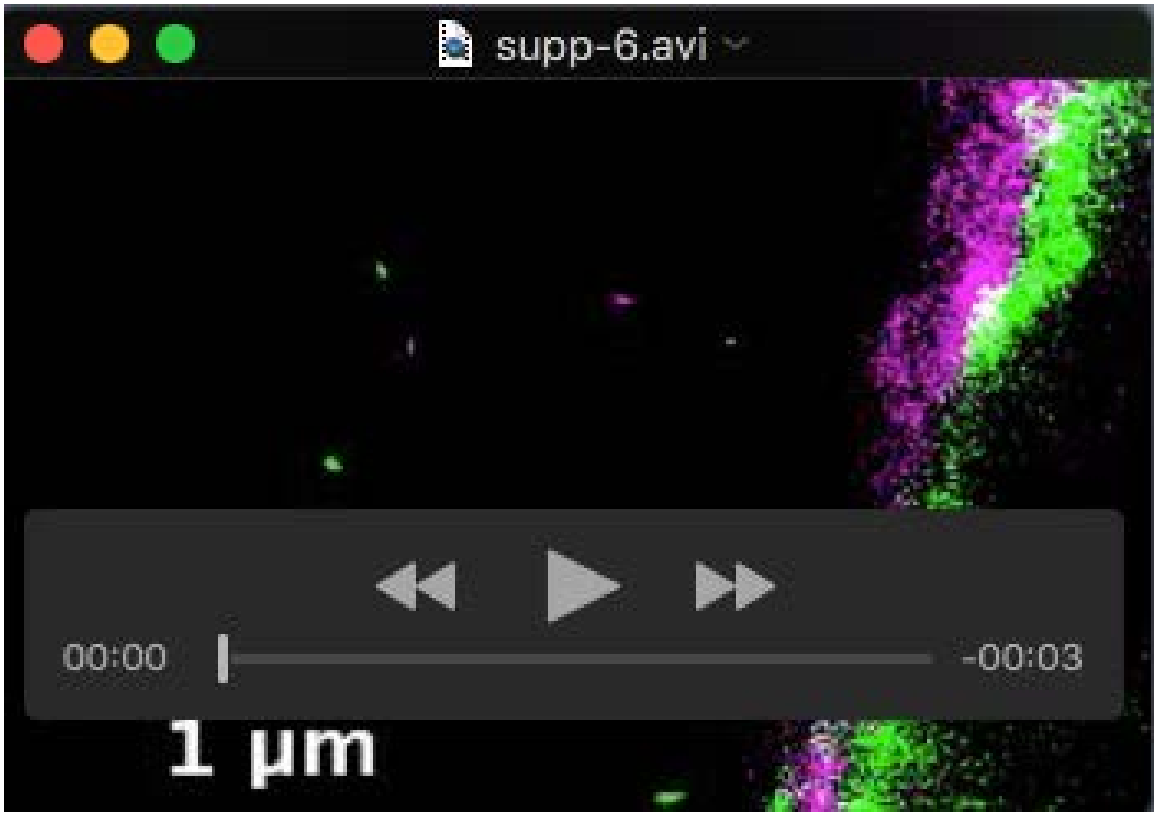

Movie S5: **Live-cell imaging of cortical actin cytoskeleton and plasma membrane reorganization during AR.** Representative super-resolution movie of a sperm loaded with SiR-actin and FM4-64 showing the formation of a hybrid vesicle at the onset of the AR. Each super-resolution image was computed by analyzing 300 wide-field images through SRRF analysis. Related to **Figure 6D-E**.

Journal of Cell Science • Supplementary information